Electronic Supplementary Material (ESI) for Dalton Transactions

Molecular rectangles from platinum(II) and bridging dicarbene, diisocyanide and 4,4'-bipyridine ligands

Markus Schmidtendorf, Tania Pape, and F. Ekkehardt Hahn*

Institut für Anorganische und Analytische Chemie, Westfälische Wilhelms-Universität Münster, Corrensstrasse 30, D-48149 Münster, Germany

Supporting Information

1. Crystals data for and molecular structures of *anti*-[6]Br_2·2MeOH·0.5C_6H_{14}, *anti*-[9]Br_2·4MeOH and *anti*-[10]Br_2·MeOH

Crystal data for *anti*-[6]Br_2·2MeOH·0.5C_6H_{14}. $C_{33}H_{69}N_4Br_4O_2P_4Pt_2$, M = 1387.62, colorless crystal, 0.27 × 0.18 × 0.10 mm^3, a = 10.2551(6), b = 12.2648(7), c = 20.1873(12) Å, , α = 77.4950(10), β = 81.3650(10), γ = 86.3760(10)°, V = 2449.5(2) Å^3, triclinic, P–1, ρ_{calcd} = 1.881 g·cm^{-3}, Mo Kα radiation, μ = 9.129 mm^{-1}, semiempirical absorption correction (0.192 ≤ T ≤ 0.462), ω- und φ-scans, 28746 measured intensities (4.4° ≤ 2θ ≤ 60.0°), 14164 independent (R_{int} = 0.0325) diffraction data, refinement of 435 parameters against all F^2, R = 0.0401, wR = 0.0998 for 11213 observed data ($I \geq 2\sigma(I)$), R_{all} = 0.0558, wR_{all} = 0.1065 for all data. The asymmetric unit contains one formula unit.

Molecular Structure of *anti*-[6]Br_2·2MeOH·0.5C_6H_{14}

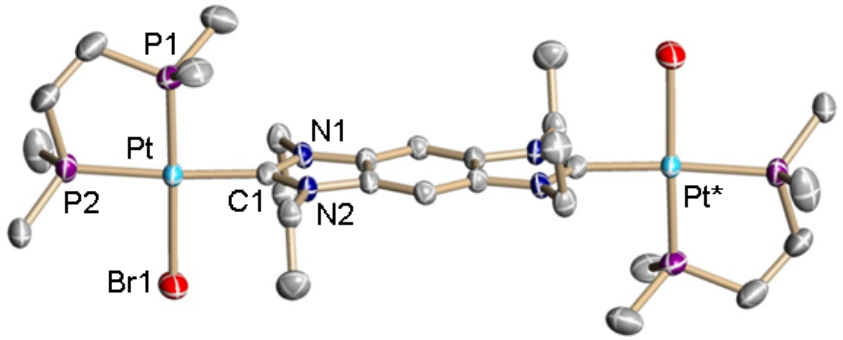

Fig. S1 Molecular structures (50% displacement ellipsoids) of the dication *anti*-[**6**]$^{2+}$ in *anti*-[**6**]Br_2·2MeOH·0.5C_6H_{14} with hydrogen atoms omitted for clarity. Selected bond lengths (Å) and angles (°): Pt–Br1 2.4845(6), Pt–P1 2.2202(15), Pt–P2 2.2823(15), Pt–C1 2.026(5); Br1–Pt–P1 177.08(5), Br1–Pt–P2 92.61(4), Br1–Pt–C1 90.52(15), P1–Pt–P2 86.2(6), P1–Pt–C1 90.78(15), P2–Pt–C1 174.8(2).

Crystal data for *anti*-[9]Br_2·4MeOH. $C_{40}H_{86}N_4Br_4O_4P_4Pt_2$, M = 1512.76, colorless crystal, 0.32 × 0.18 × 0.16 mm^3, a = 11.4288(8), b = 10.7546(7), c = 24.763(2) Å, β = 99.2950(10)°, V = 3003.7(4) Å^3, monoclinic, $P2_1/c$, Z = 2, ρ_{calcd} = 1.673 g·cm^{-3}, Mo Kα radiation, μ = 7.455 mm^{-1}, semiempirical absorption correction ($0.199 \le T \le 0.382$), ω- und φ-scans, 27935 measured intensities ($3.3° \le 2\theta \le 58.0°$), 7936 independent ($R_{int}$ = 0.0377) diffraction data, refinement of 271 parameters against all F^2, R = 0.0402, wR = 0.0972 for 6397 observed data ($I \ge 2\sigma(I)$), R_{all} = 0.0543, wR_{all} = 0.1036 for all data. The asymmetric unit contains ½ formula unit related to the other half by a crystallographic inversion center.

Molecular Structure of *anti*-[9]Br_2·4MeOH

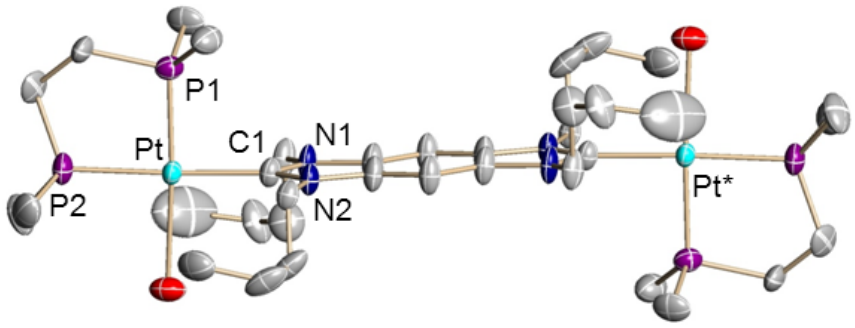

Fig. S2 Molecular structures (50% displacement ellipsoids) of the dication *anti*-[**9**]$^{2+}$ in *anti*-[**6**]Br_2·4MeOH with hydrogen atoms omitted for clarity. Selected bond lengths (Å) and angles (°): Pt–Br1 2.4831(7), Pt–P1 2.2228(15), Pt–P2 2.2680(15), Pt–C1 2.039(5); Br1–Pt–P1 176.17(4), Br1–Pt–P2 90.58(5), Br1–Pt–C1 92.1(2), P1–Pt–P2 86.15(6), P1–Pt–C1 91.2(2), P2–Pt–C1 177.1(2).

Crystal data for *anti*-[10]Br_2·MeOH. $C_{37}H_{74}N_4Br_4OP_4Pt_2$, M = 1424.70, colorless crystal, 0.19 × 0.10 × 0.05 mm^3, a = 11.4812(5), b = 10.8653(5), c = 21.0825(10) Å, β = 93.9670(10)°, V = 2623.7(2) Å^3, monoclinic, $P2_1/c$, Z = 2, ρ_{calcd} = 1.803 g·cm^{-3}, Mo Kα radiation, μ = 8.524 mm^{-1}, semiempirical absorption correction ($0.294 \le T \le 0.675$), ω- und φ-scans, 28853 measured intensities ($3.6° \le 2\theta \le 60.0°$), 7577 independent ($R_{int}$ = 0.0403) diffraction data, refinement of 254 parameters against all F^2, R = 0.0358, wR = 0.0878 for 6316 observed data ($I \ge 2\sigma(I)$), R_{all} = 0.0470, wR_{all} = 0.0927 for all data. The asymmetric unit contains ½ formula unit related to the other half by a crystallographic inversion center.

Molecular Structure of *anti*-[10]Br_2·MeOH

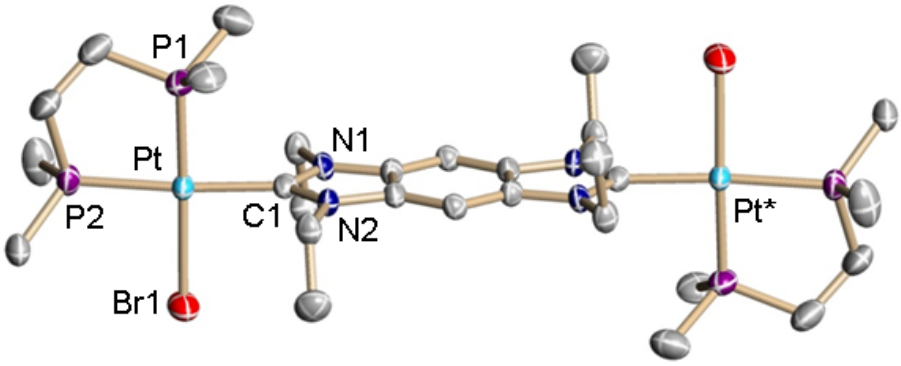

Fig. S3 Molecular structures (50% displacement ellipsoids) of the dication *anti*-[**10**]$^{2+}$ in *anti*-[**6**]Br_2·MeOH with hydrogen atoms omitted for clarity. Selected bond lengths (Å) and angles (°): Pt–Br1 2.5093(5), Pt–P1 2.2225(13), Pt–P2 2.2831(12), Pt–C1 2.040(5); Br1–Pt–P1 174.53(3), Br1–Pt–P2 88.79(4), Br1–Pt–C1 93.49(12), P1–Pt–P2 85.75(5), P1–Pt–C1 91.98(13), P2–Pt–C1 176.20(13).

2. ^{1}H and ^{13}C NMR spectra for all new compounds

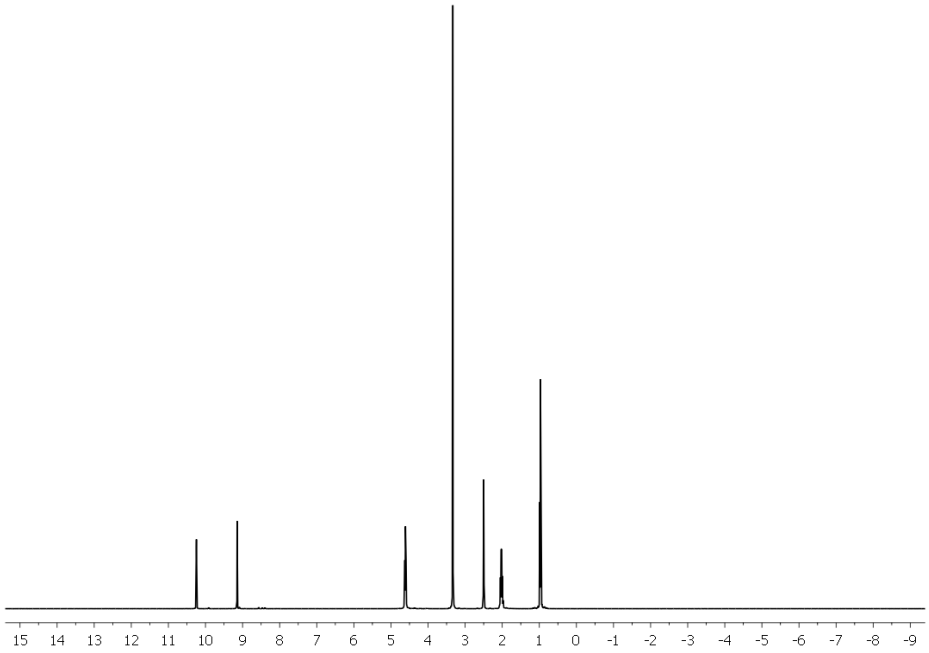

Fig. S4 ^{1}H-NMR spectrum of **2**-Br_2 in D_6-DMSO.

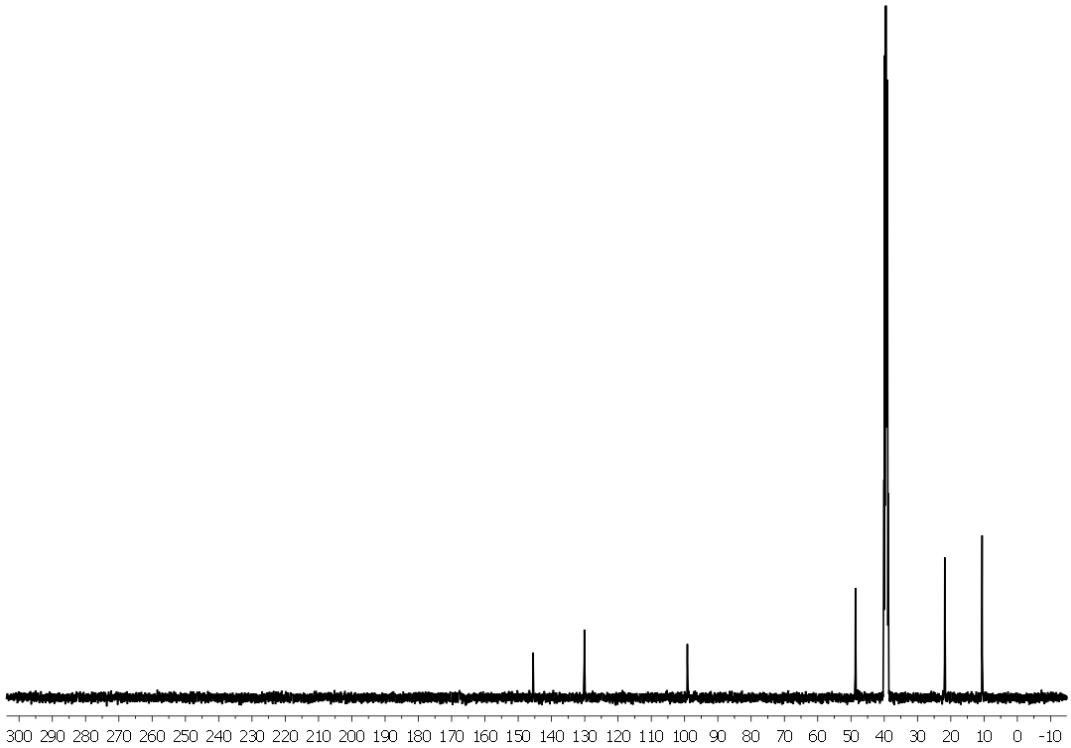

Fig. S5 ^{13}C{^{1}H}-NMR spectrum of **2**-Br_2 in D_6-DMSO.

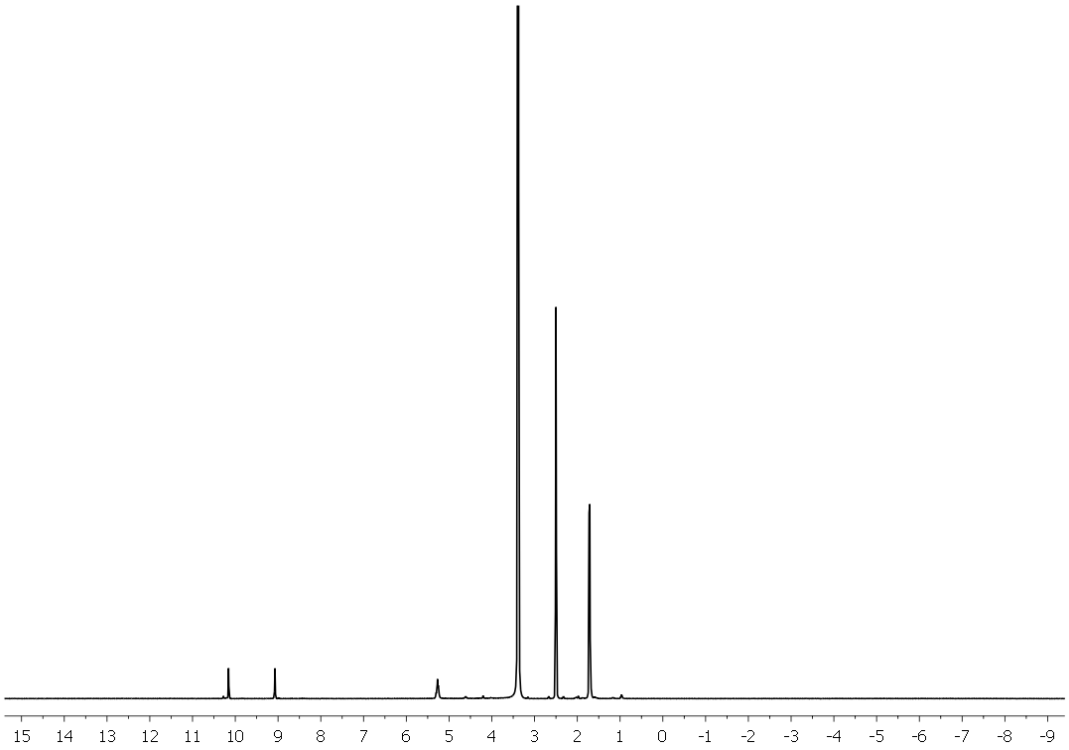

Fig. S6 ^{1}H-NMR spectrum of **3**-Br_2 in D_6-DMSO.

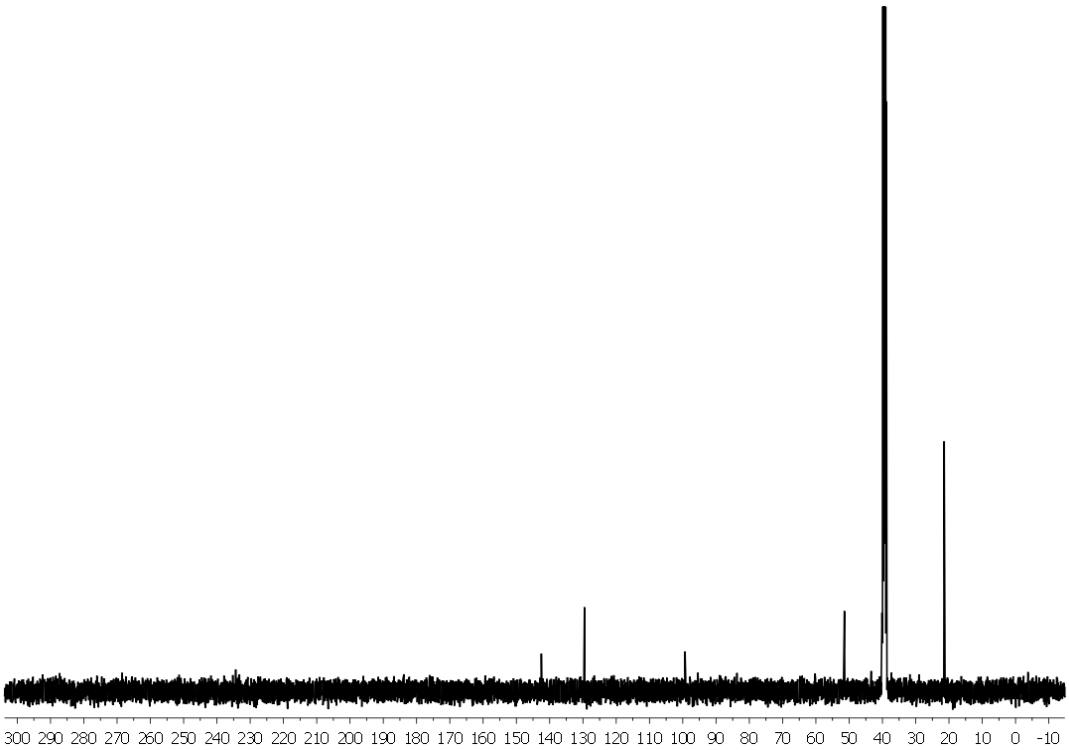

Fig. S7 $^{13}C\{^{1}H\}$-NMR spectrum of **3**-Br_2 in D_6-DMSO.

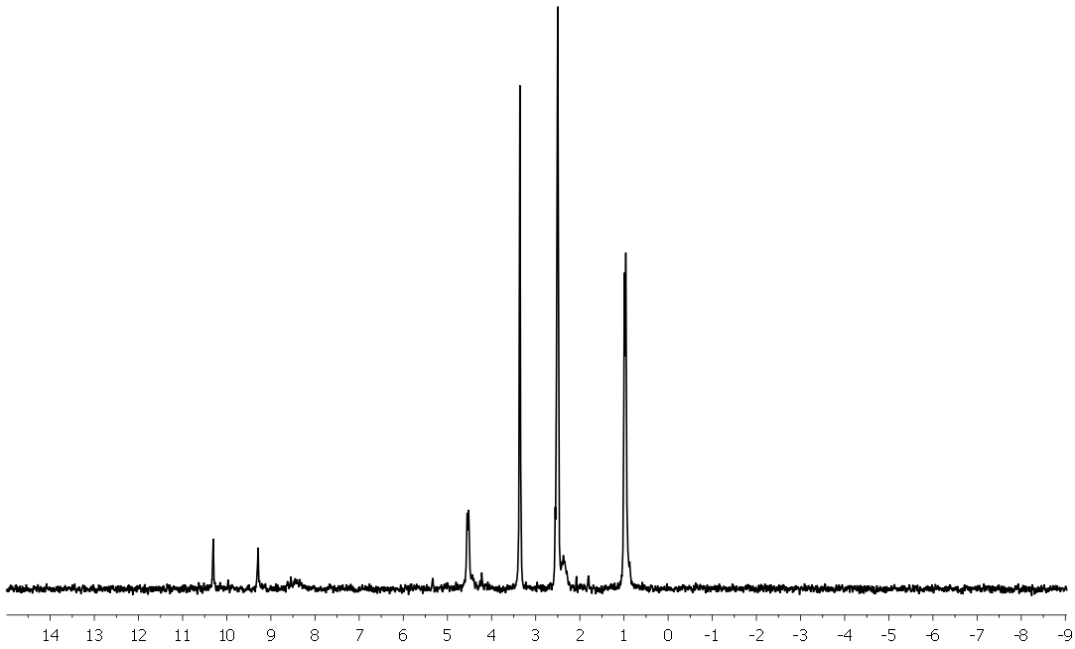

Fig. S8 ^{1}H-NMR spectrum of **4**-Br_2 in D_6-DMSO.

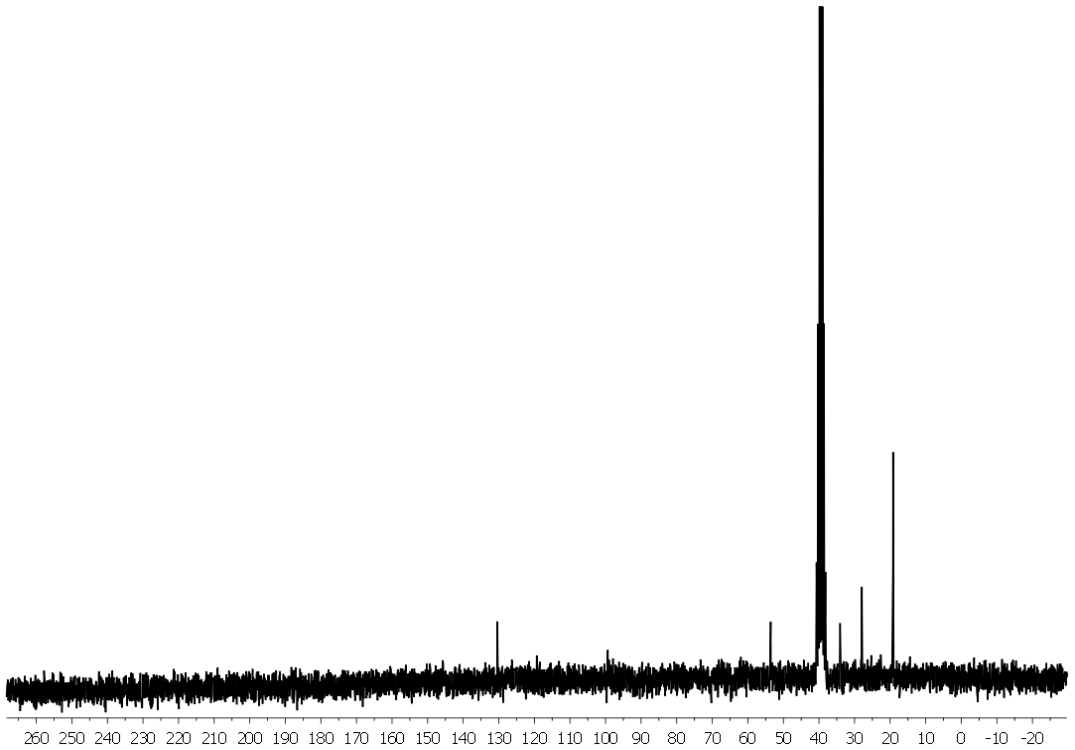

Fig. S9 $^{13}C\{^{1}H\}$-NMR spectrum of **4**-Br_2 in D_6-DMSO.

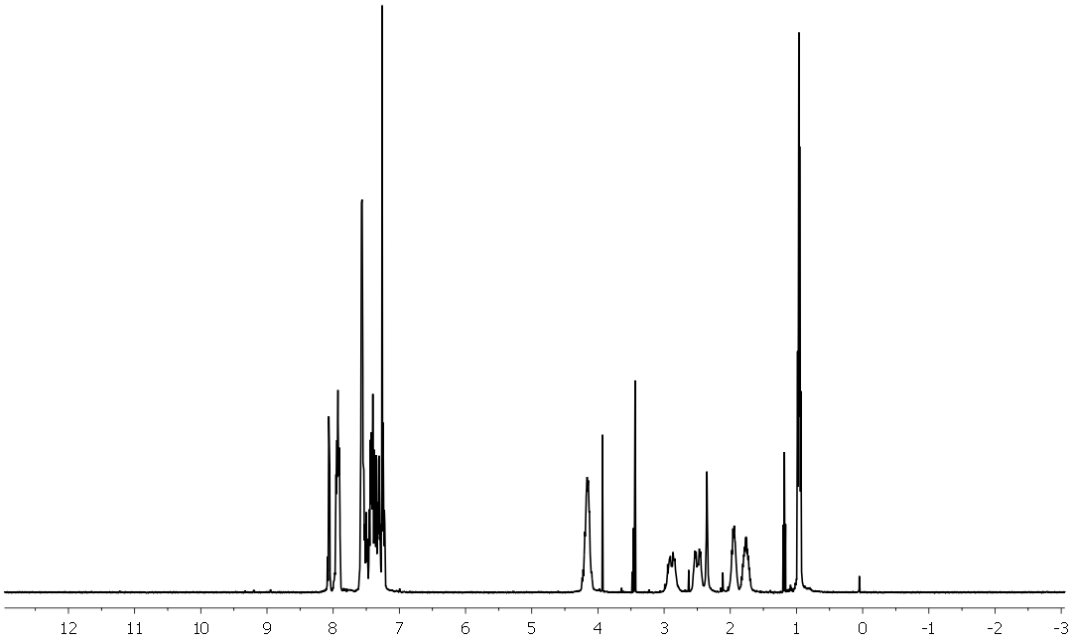

Fig. S10 ^{1}H-NMR spectrum of a mixture of *syn*/*anti*-[**5**]Br_2 in $CDCl_3$.

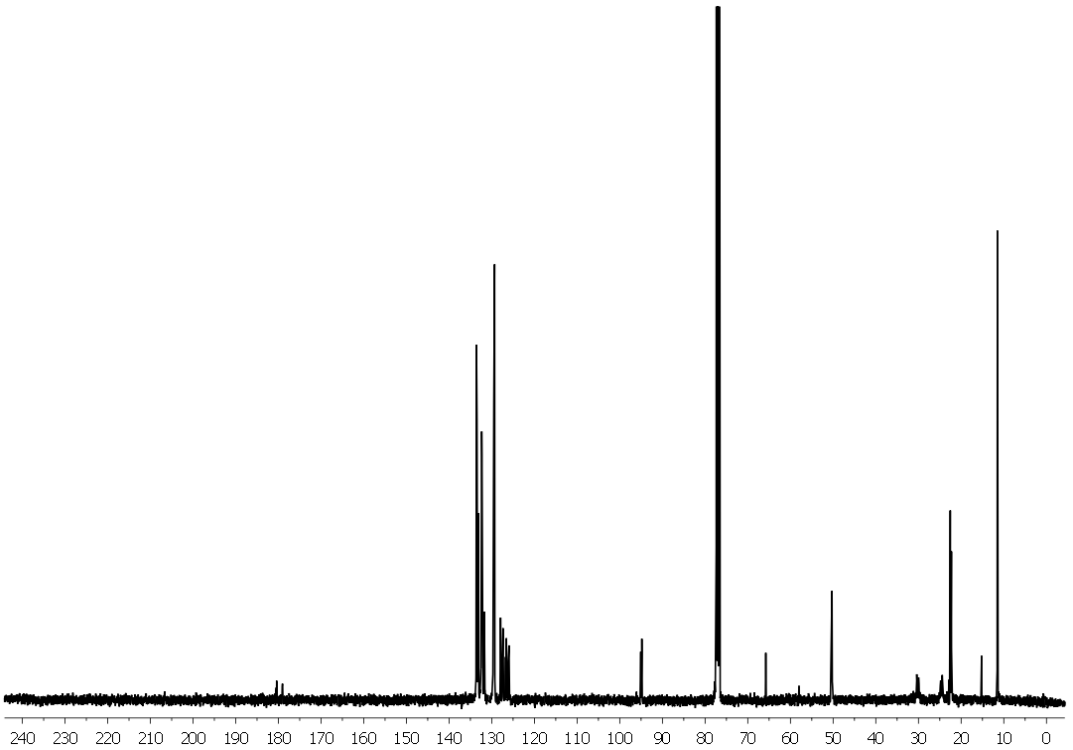

Fig. S11 $^{13}C\{^{1}H\}$-NMR spectrum of a mixture of *syn*/*anti*-[**5**]Br_2 in $CDCl_3$.

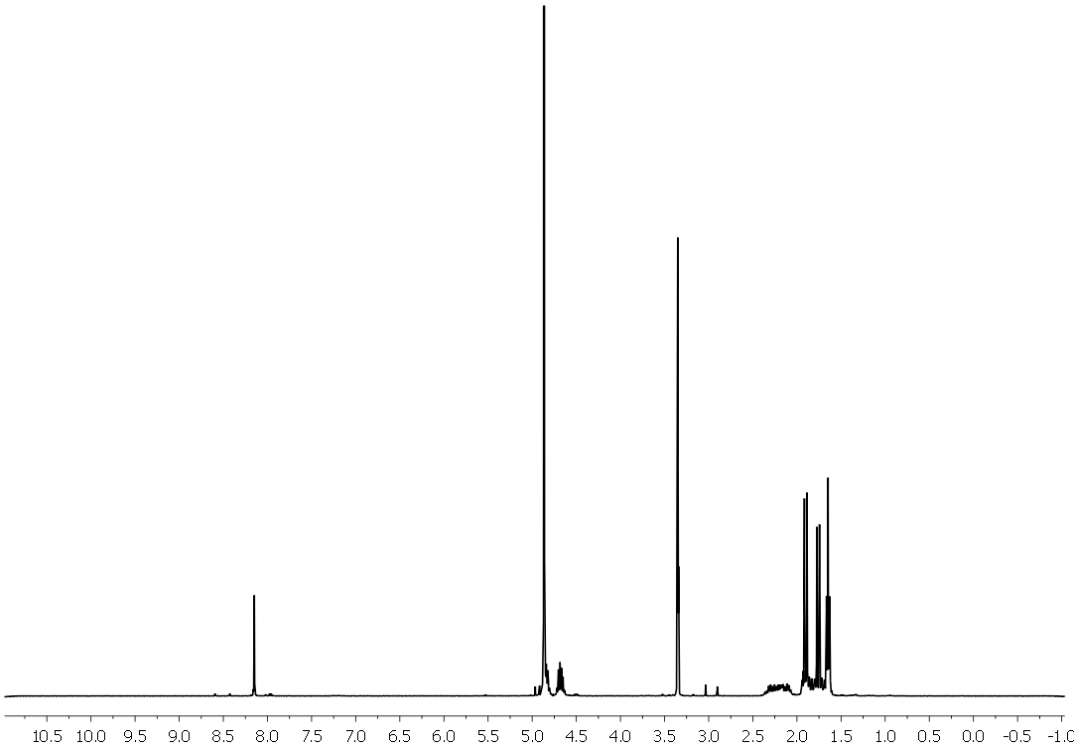

Fig. S12 ^{1}H-NMR spectrum of [**6**]Br_2 in CD_3OD.

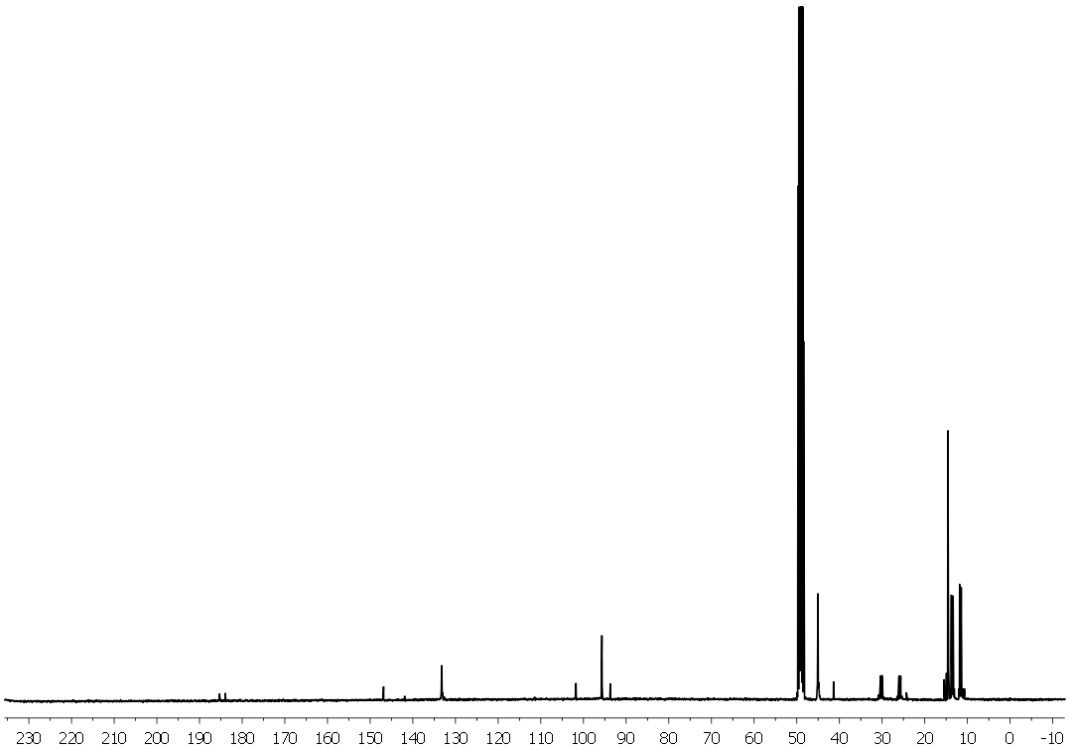

Fig. S13 $^{13}C\{^{1}H\}$-NMR spectrum of [**6**]Br_2 in CD_3OD.

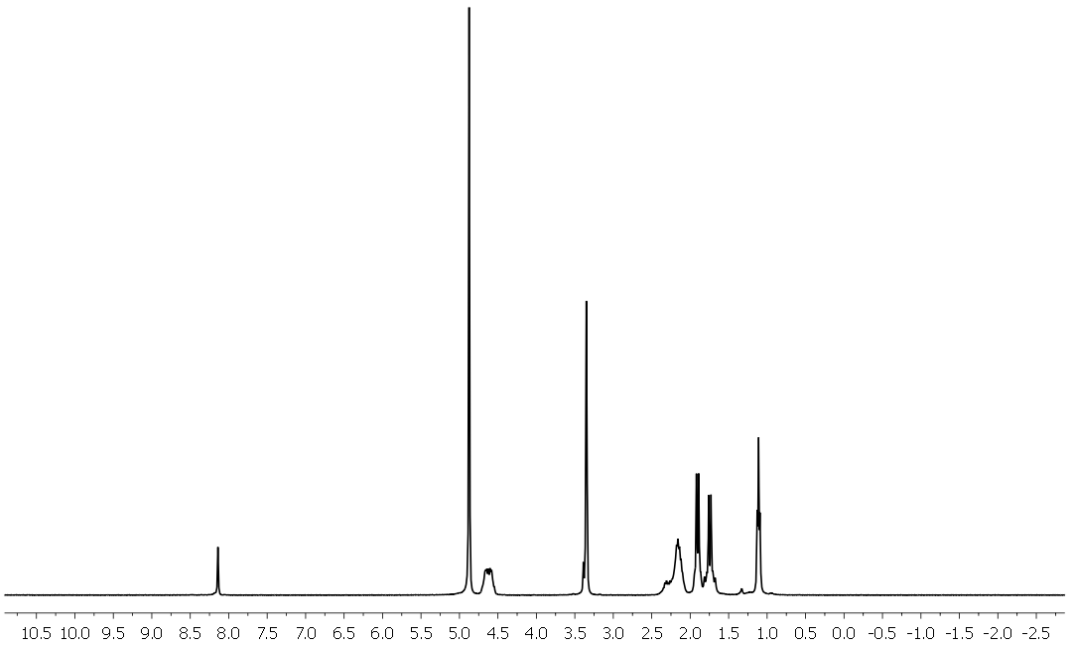

Fig. S14 ^{1}H-NMR spectrum of [**7**]Br_2 in CD_3OD.

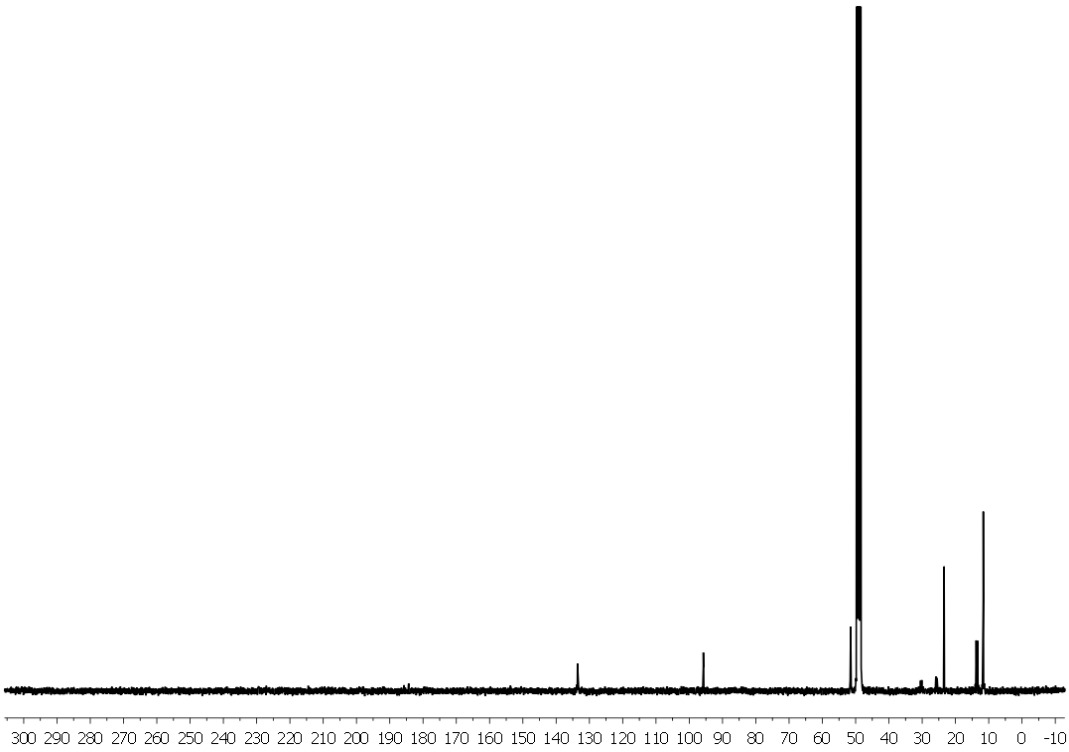

Fig. S15 $^{13}C\{^{1}H\}$-NMR spectrum of [**7**]Br_2 in CD_3OD.

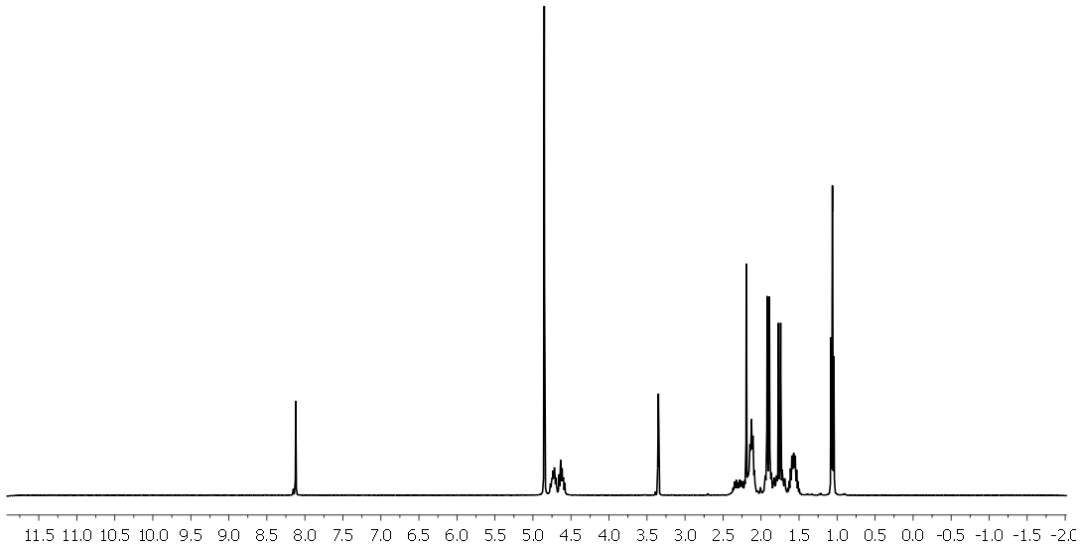

Fig. S16 ^{1}H-NMR spectrum of [**9**]Br_2 in CD_3OD.

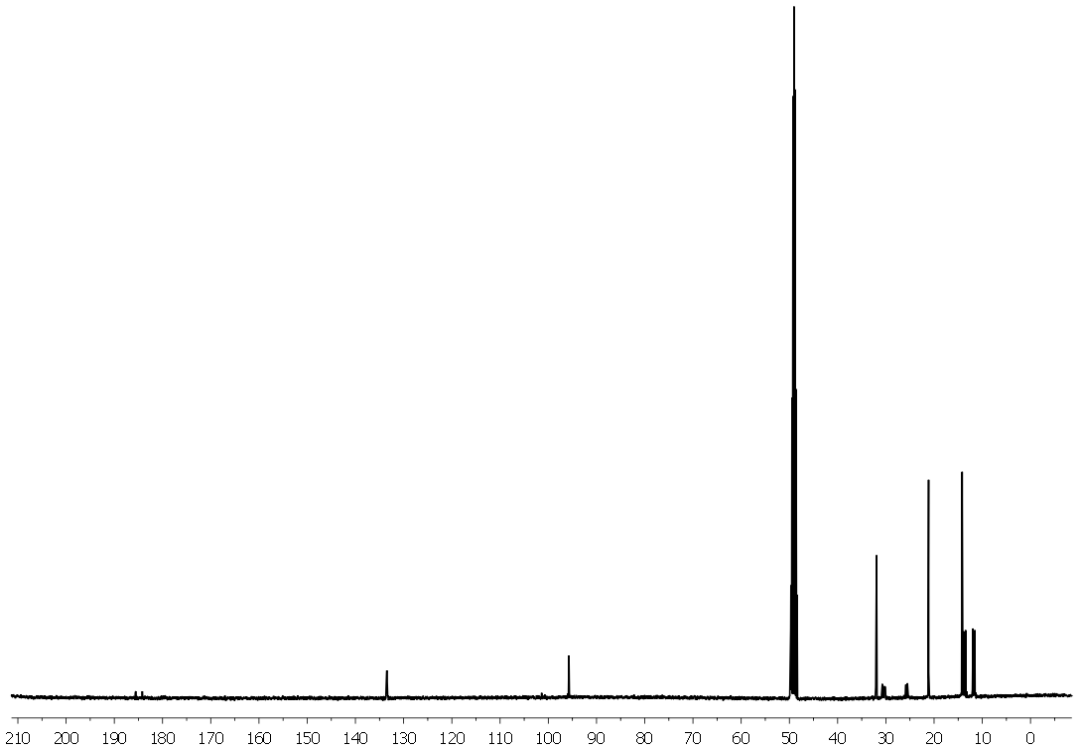

Fig. S17 $^{13}C\{^{1}H\}$-NMR spectrum of [**9**]Br_2 in CD_3OD.

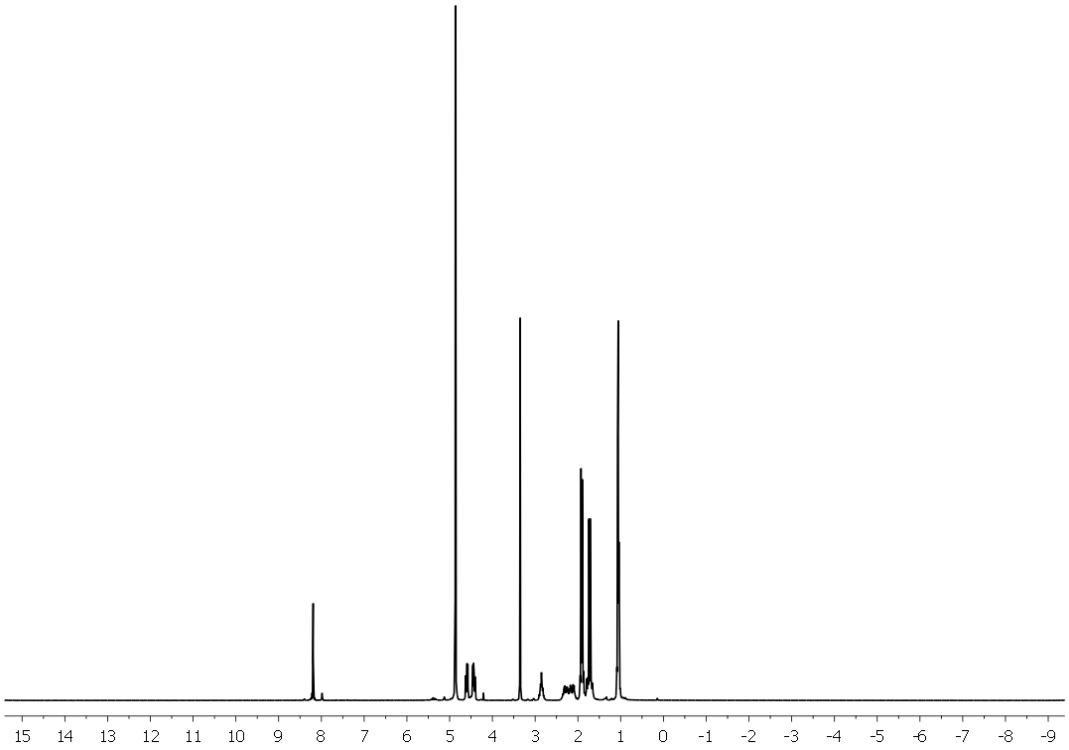

Fig. S18 ^{1}H-NMR spectrum of [**10**]Br_2 in CD_3OD.

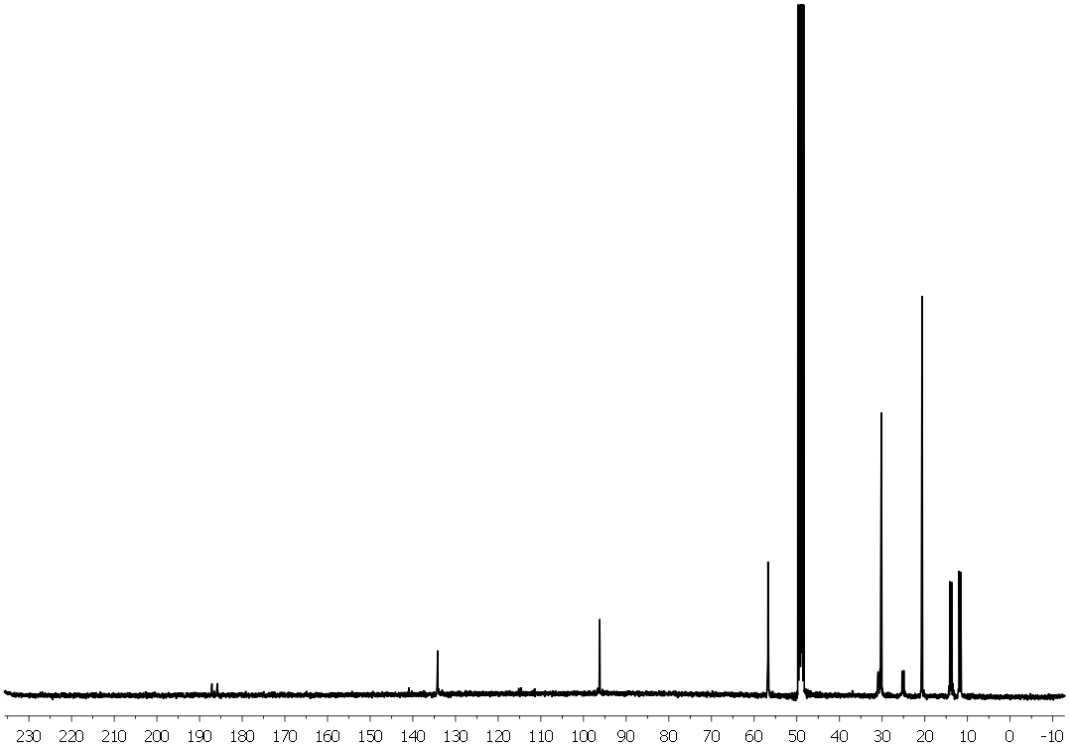

Fig. S19 $^{13}C\{^{1}H\}$-NMR spectrum of [**10**]Br_2 in CD_3OD.

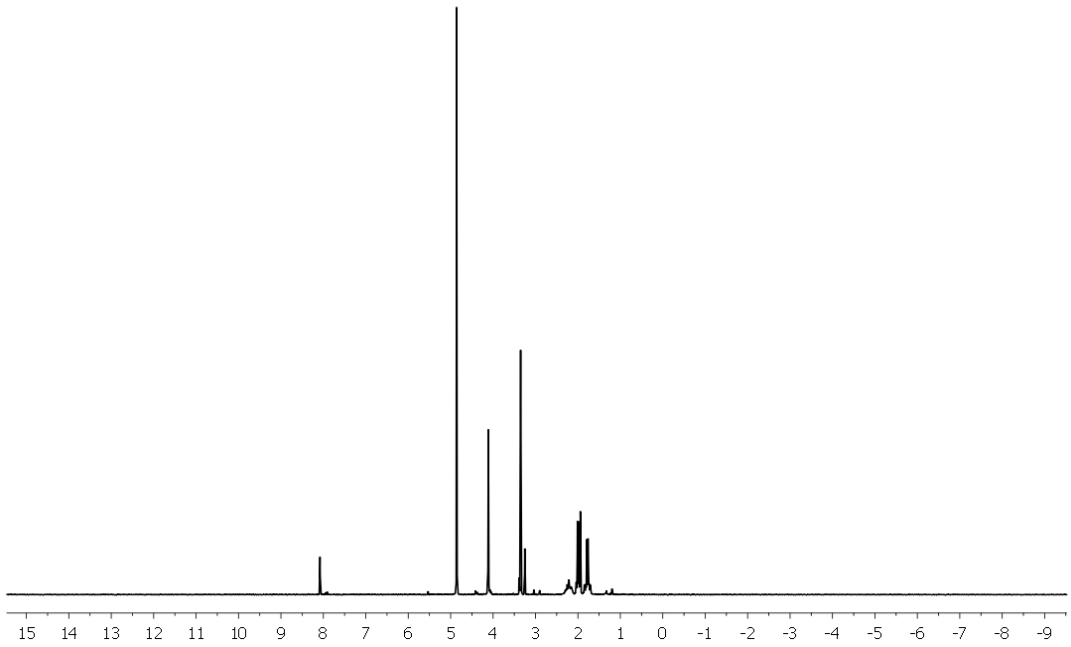

Fig. S20 ^{1}H-NMR spectrum of [**11**]I_2 in CD_3OD.

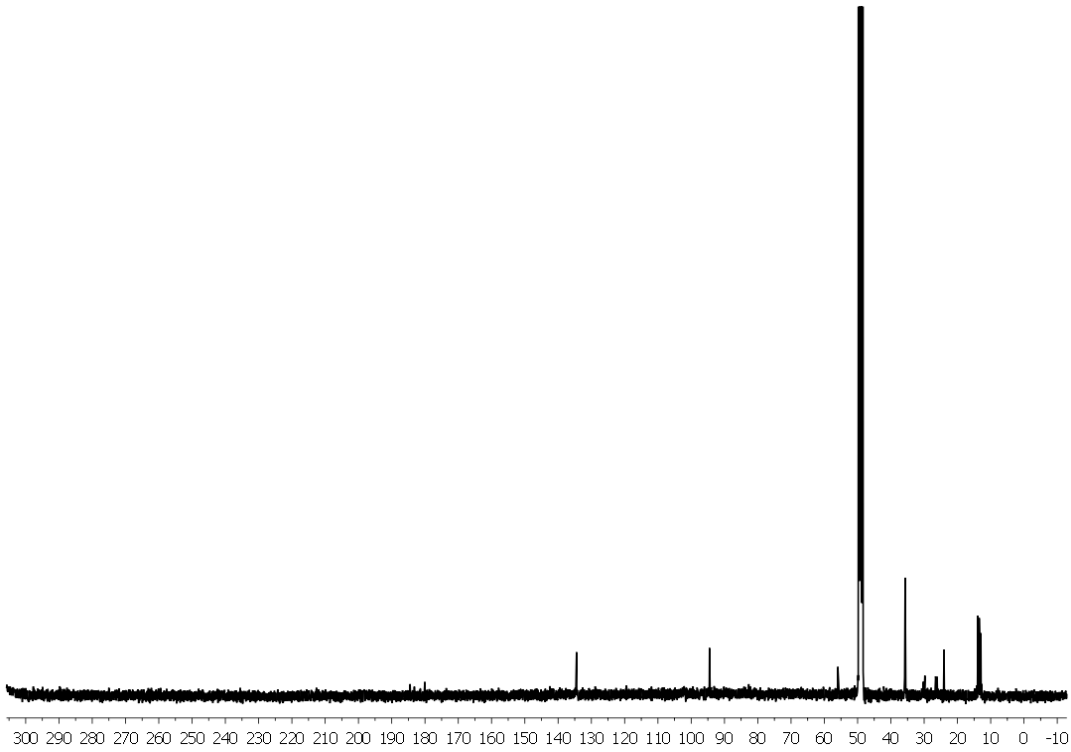

Fig. S21 $^{13}C\{^{1}H\}$-NMR spectrum of [**11**]I_2 in CD_3OD.

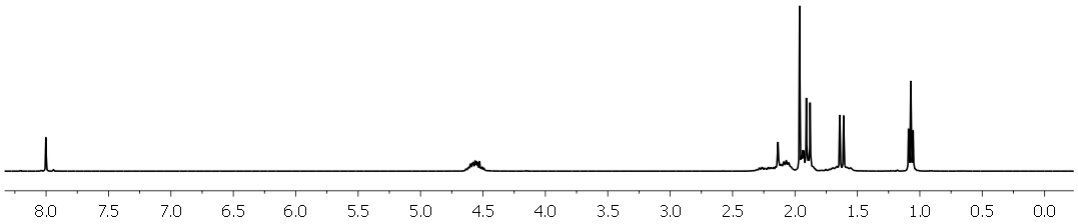

Fig. S22 ^{1}H-NMR spectrum of [**12**]$(PF_6)_4$ in CD_3CN.

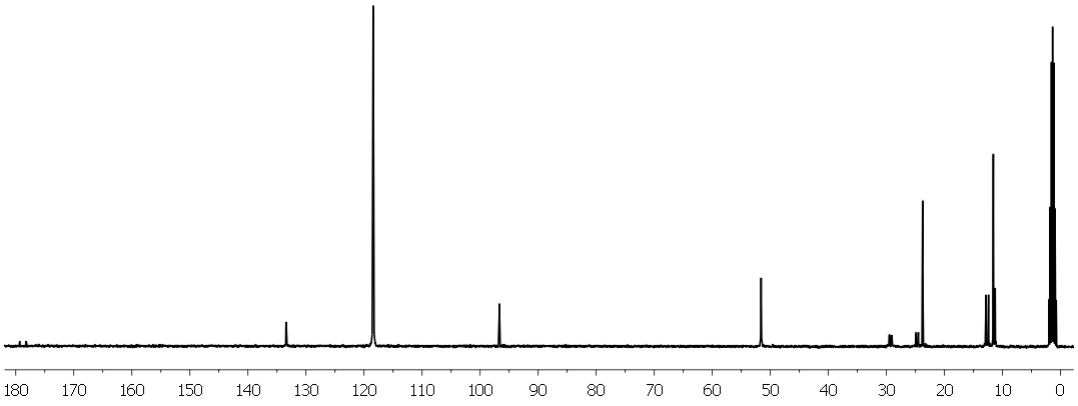

Fig. S23 $^{13}C\{^{1}H\}$-NMR spectrum of [**12**]$(PF_6)_4$ in CD_3CN.

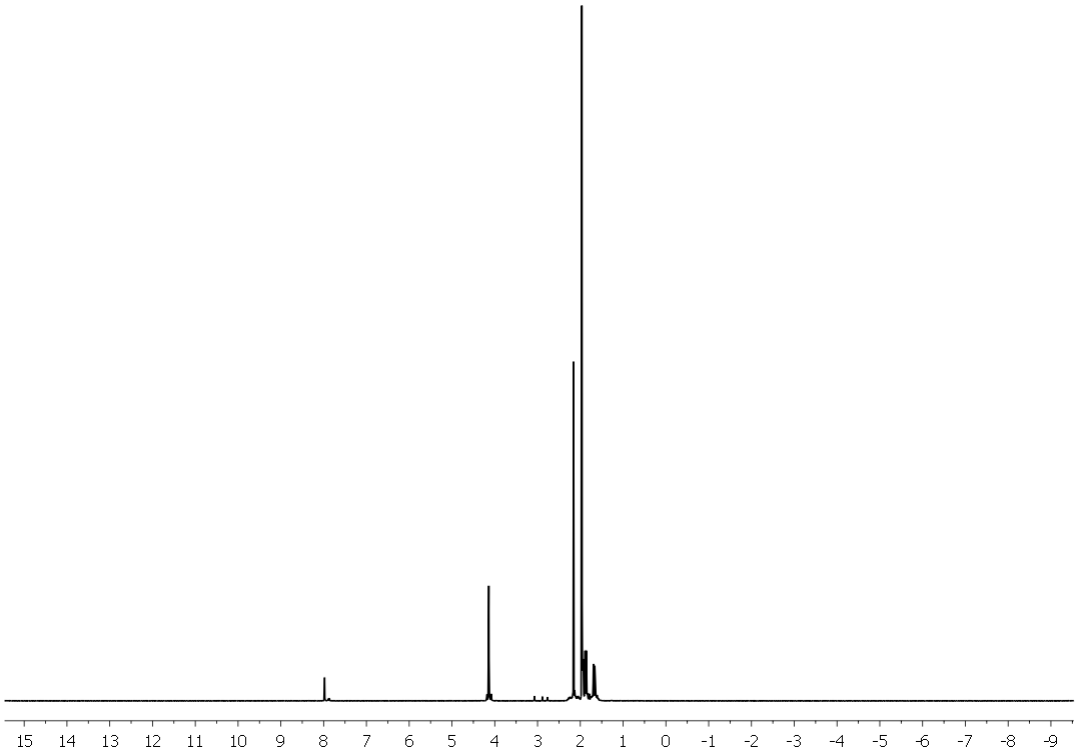

Fig. S24 ^{1}H-NMR spectrum of [**13**](PF$_6$)$_4$ in CD$_3$CN.

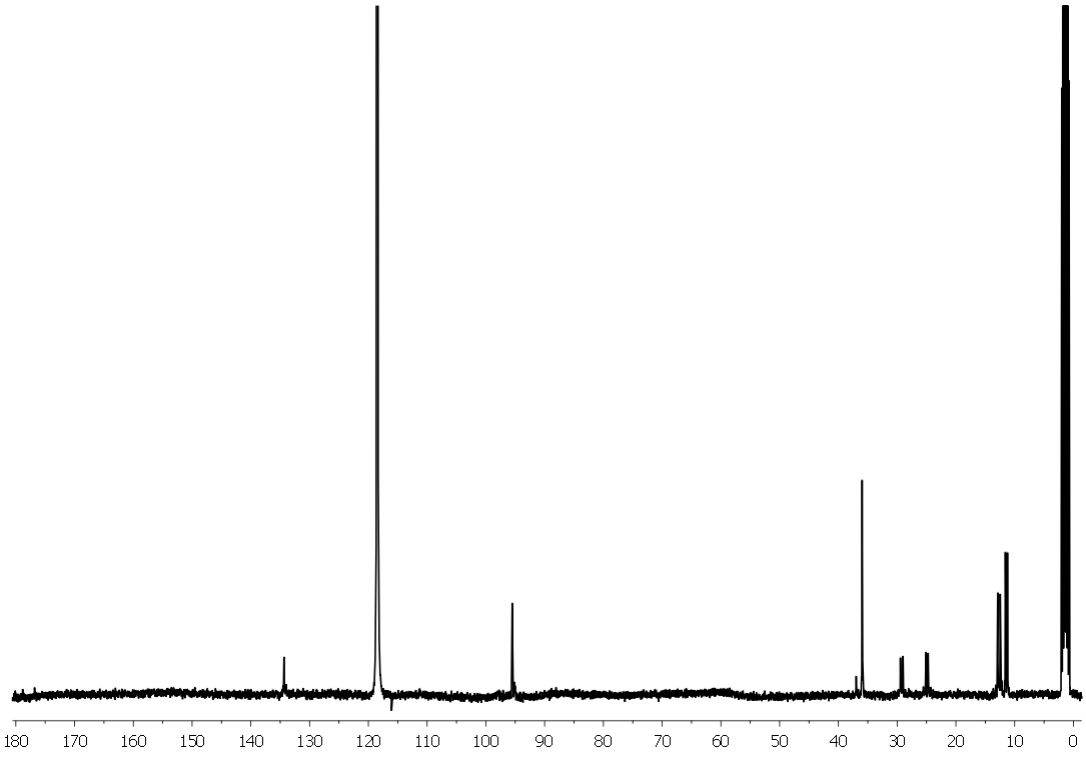

Fig. S25 ^{13}C{^{1}H}-NMR spectrum of [**13**](PF$_6$)$_4$ in CD$_3$CN.

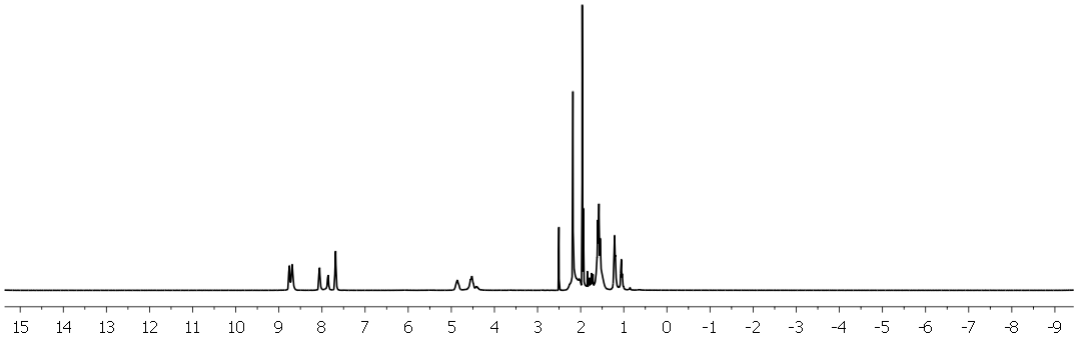

Fig. S26 ^{1}H-NMR spectrum of [**14**](PF$_6$)$_4$ in CD$_3$CN.

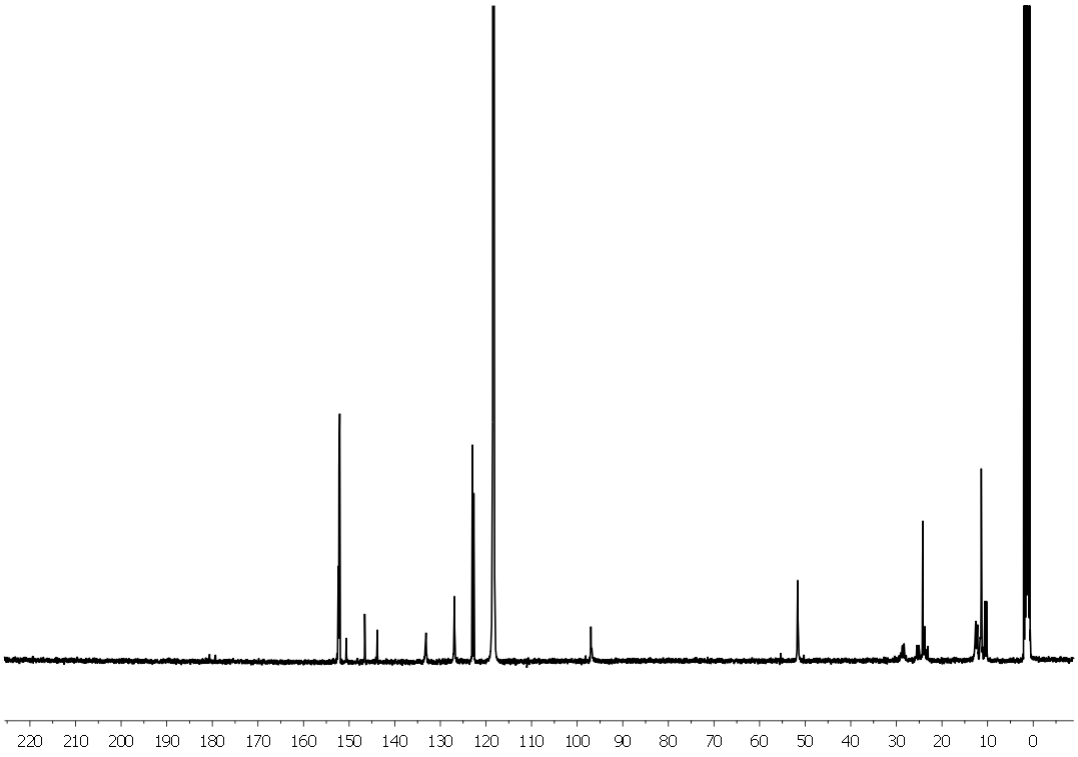

Fig. S27 ^{13}C{^{1}H}-NMR spectrum of [**14**](PF$_6$)$_4$ in CD$_3$CN.

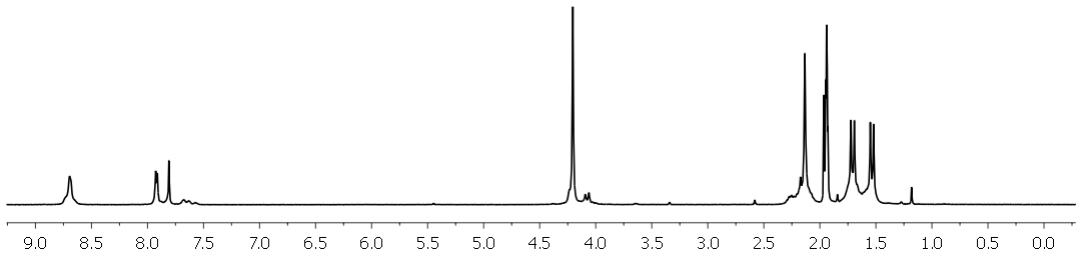

Fig. S28 ^{1}H-NMR spectrum of [**15**](PF$_6$)$_8$ in CD$_3$CN.

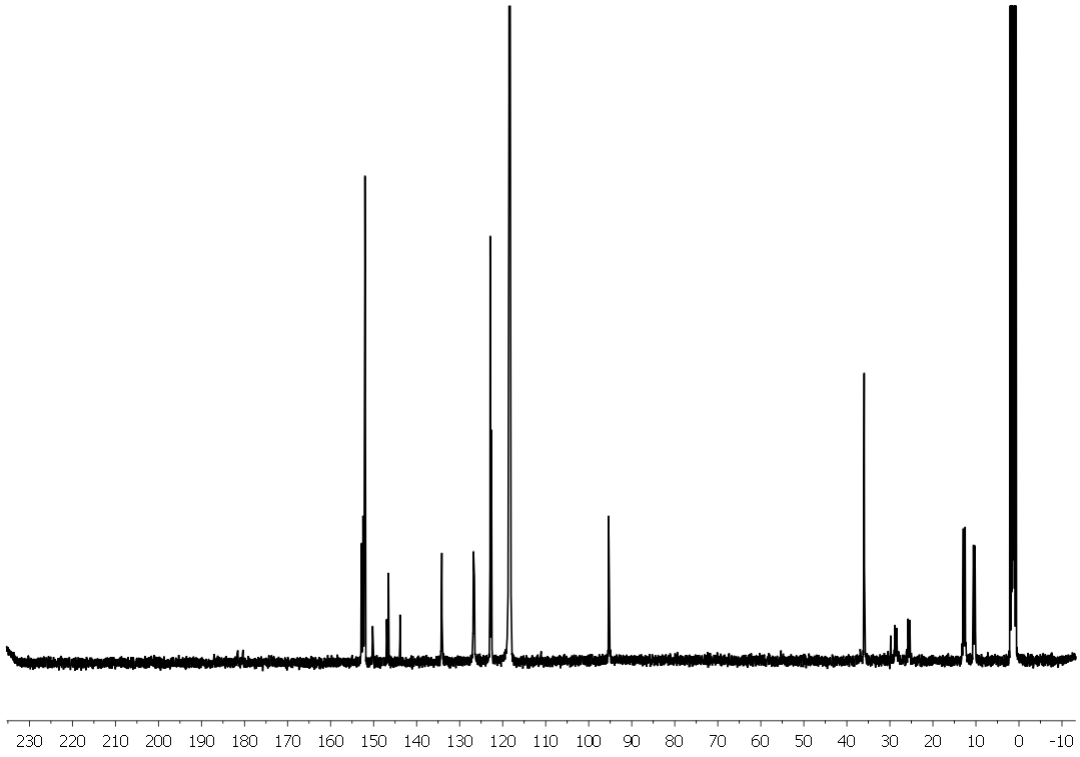

Fig. S29 ^{13}C{^{1}H}-NMR spectrum of [**15**](PF$_6$)$_8$ in CD$_3$CN.

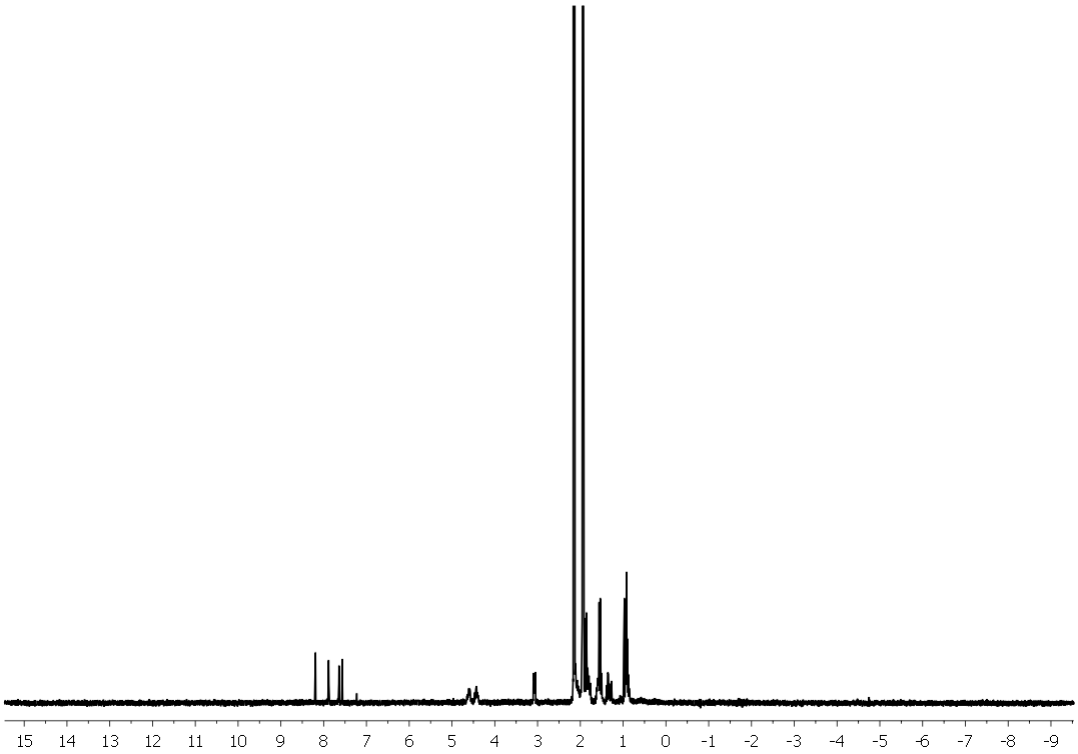

Fig. S30 ^{1}H-NMR spectrum of [**17**](BF$_4$)$_4$ in CD$_3$CN.

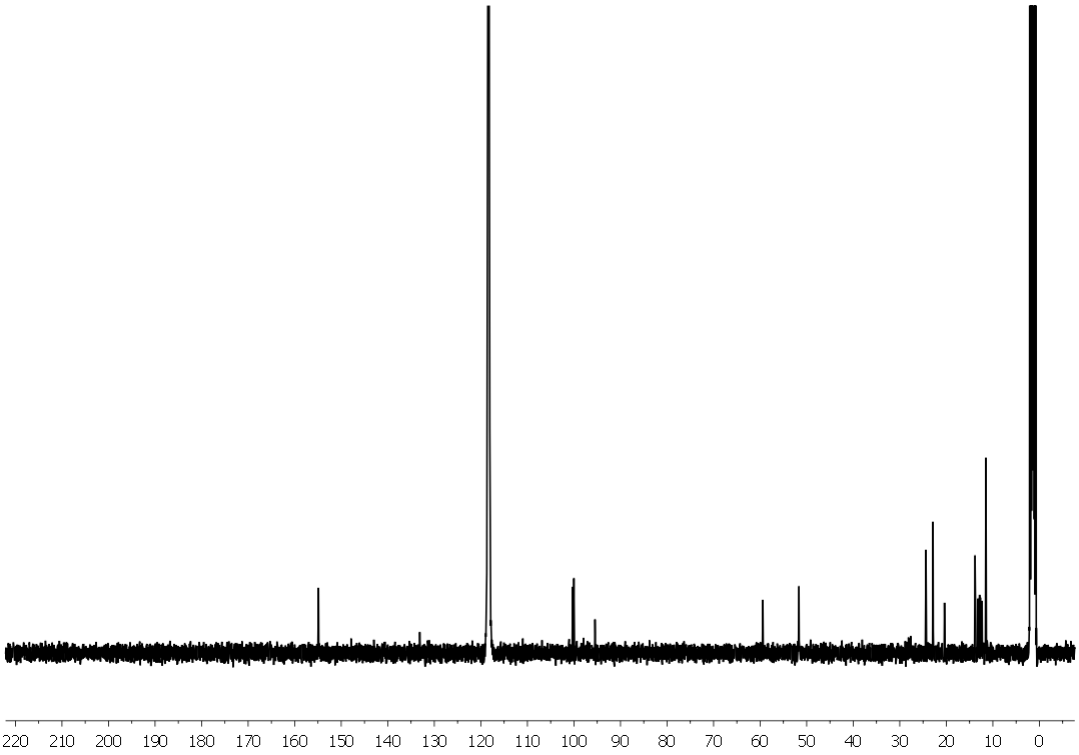

Fig. S31 ^{13}C{^{1}H}-NMR spectrum of [**17**](BF$_4$)$_4$ in CD$_3$CN.

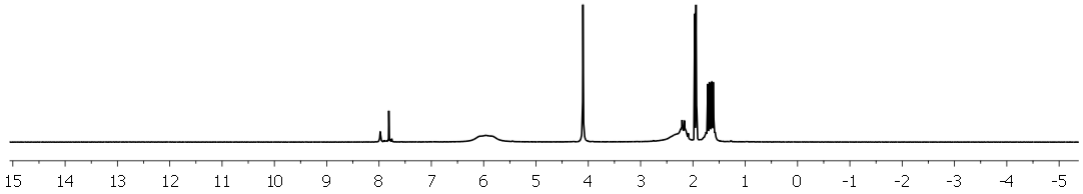

Fig. S32 ^{1}H-NMR spectrum of [**18**](BF$_4$)$_8$ in CD$_3$CN.

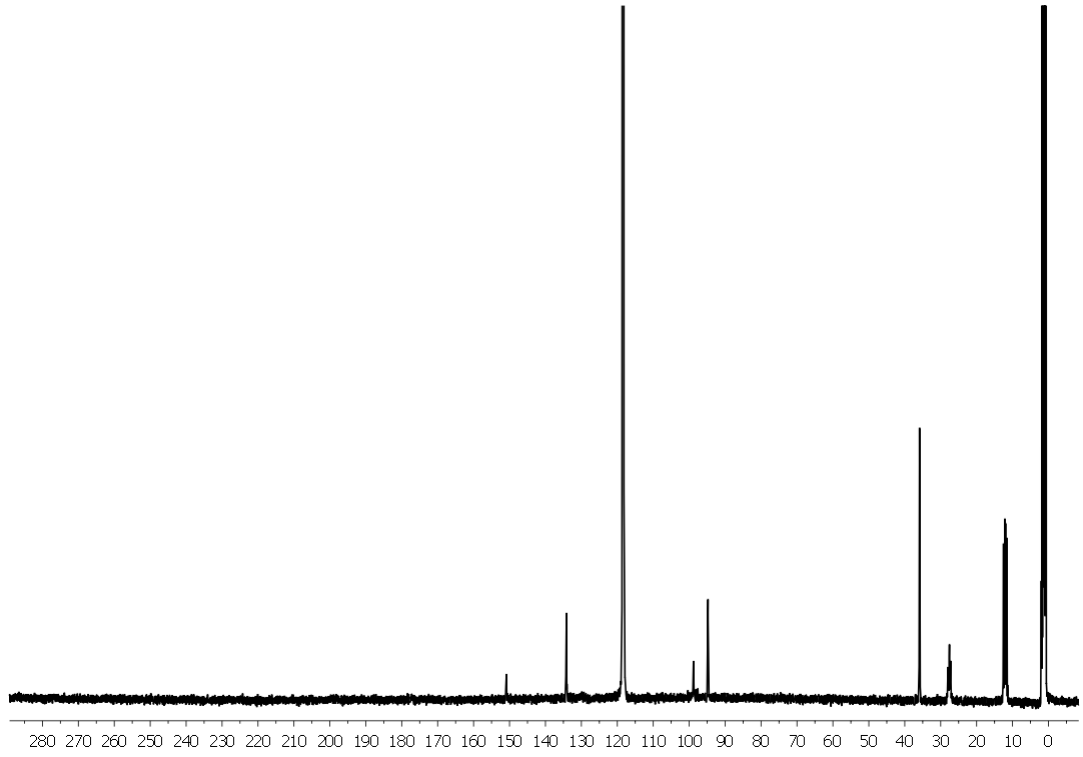

Fig. S33 ^{13}C{^{1}H}-NMR spectrum of [**18**](BF$_4$)$_8$ in CD$_3$CN.

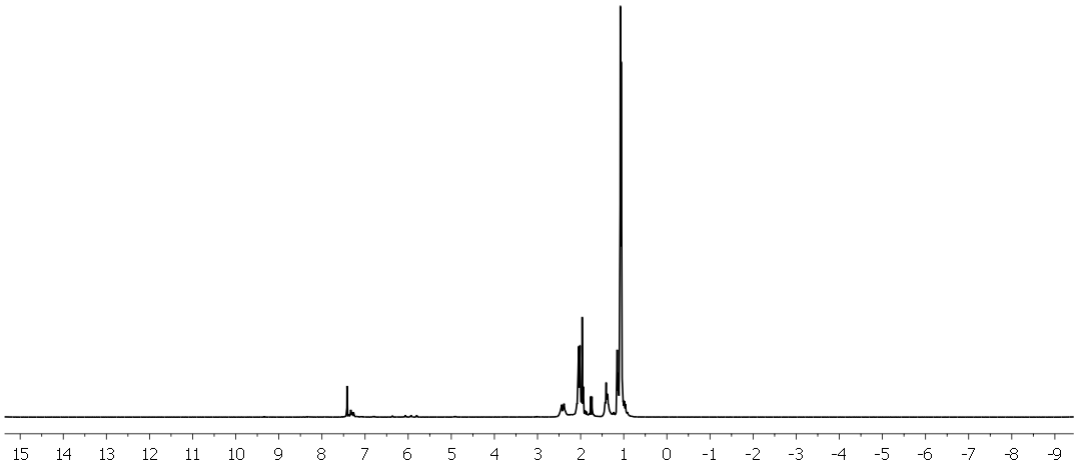

Fig. S34 ^{1}H-NMR spectrum of [**19**](BF$_4$)$_8$ in CD$_3$CN.

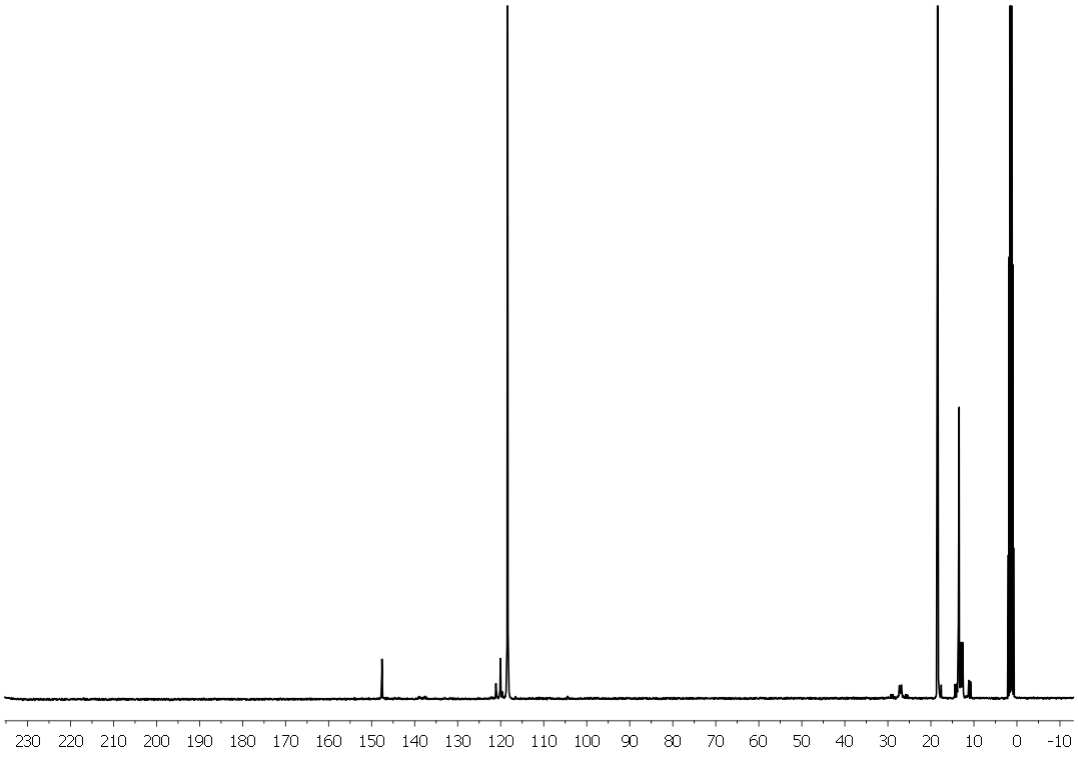

Fig. S35 ^{13}C{^{1}H}-NMR spectrum of [**19**](BF$_4$)$_8$ in CD$_3$CN.

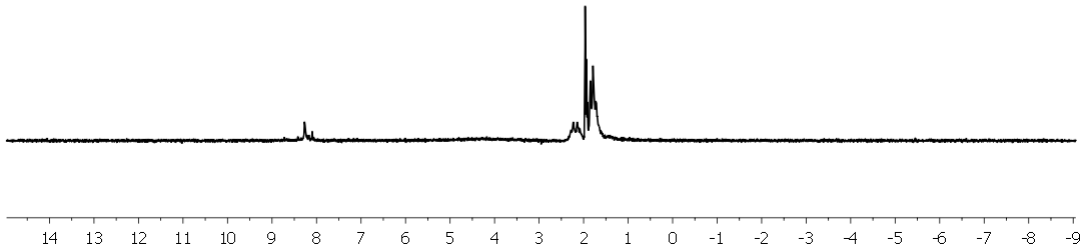

Fig. S36 ^{1}H-NMR spectrum of [**20**](BF$_4$)$_8$ in CD$_3$CN.

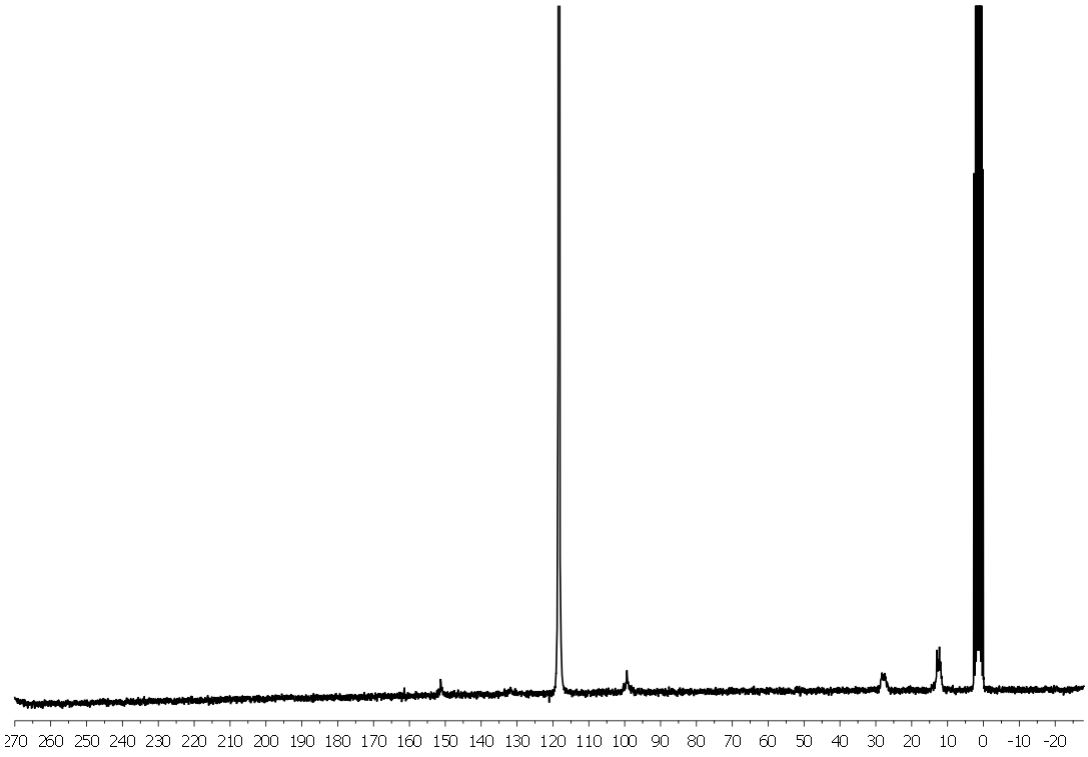

Fig. S37 ^{13}C{^{1}H}-NMR spectrum of [**20**](BF$_4$)$_8$ in CD$_3$CN.